Supplementary Materials

Defect-engineered Metal-Organic Framework (MOF-808) towards the Improved Adsorptive Removal of Organic Dyes and Chromium (VI) Species from Water

Khoa D. Nguyen, [a,b] Nhi T. Vo, [a,b] Khanh T. M. Le, [a,b] Khanh V. Ho, [a,b] Nam T. S. Phan, [a,b] Phuoc H. Ho, [c]* Ha V. Le [a,b]*

[a] Department of Chemical Engineering, Ho Chi Minh University of Technology (HCMUT), 268 Ly Thuong Kiet street, District 10, Ho Chi Minh City, 70000 Vietnam.

[b] Vietnam National University Ho Chi Minh city, Linh Trung Ward, Ho Chi Minh City, 70000 Vietnam.

[c] Chemical Engineering, Competence Centre for Catalysis, Chalmers University of Technology, Gothenburg, SE-412 96, Sweden.

Corresponding Authors

* E-mail: phuoc@chalmers.se (Phuoc. H. Ho); and lvha@hcmut.edu.vn (Ha V. Le)

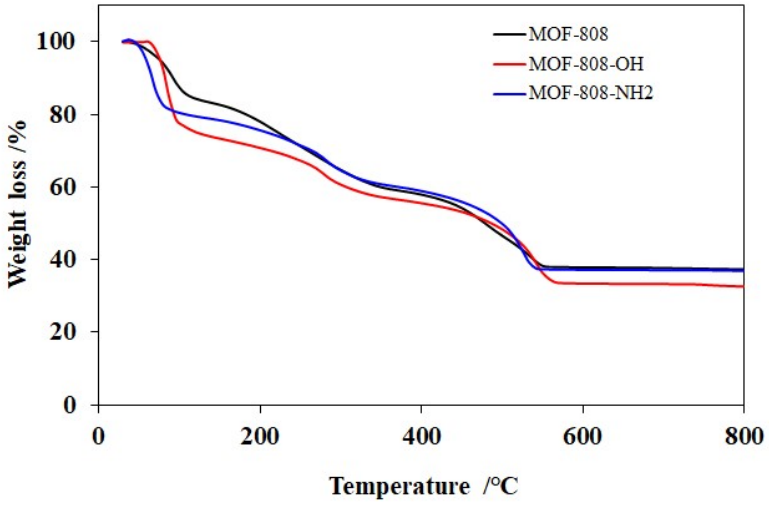

Figure S1. TGA profiles of the pristine and defective MOF-808.

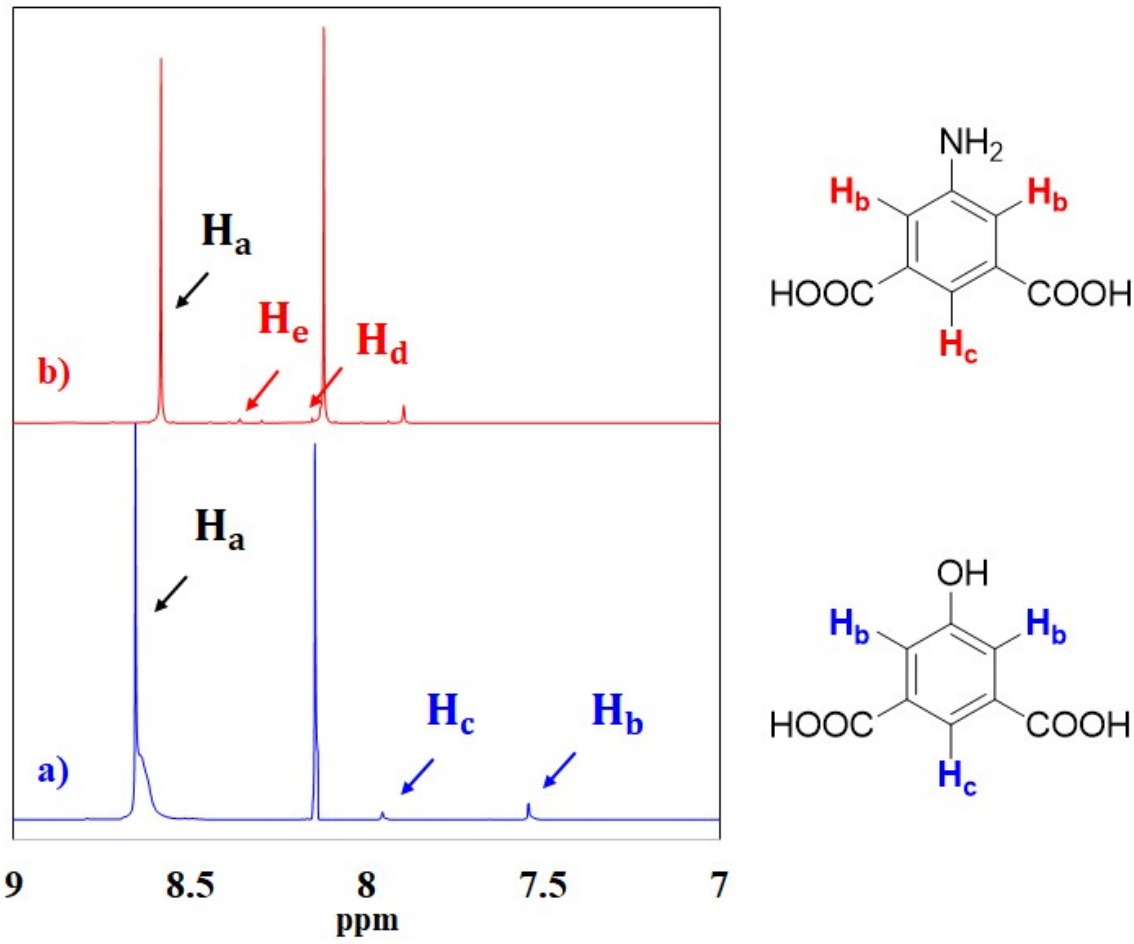

Figure S2. NMR spectra of defective MOF-808 analogues as employing 50 mol% of defective inducers.

Table S1. Maximum adsorption wavelength of organic dyes and potassium dichromate.

Adsorbate	Maximum adsorption wavelength (nm)
Sunset yellow	482
Quinoline yellow	441
Methyl orange	464
Methylene blue	664
Malachite green	618
Potassium dichromate	351

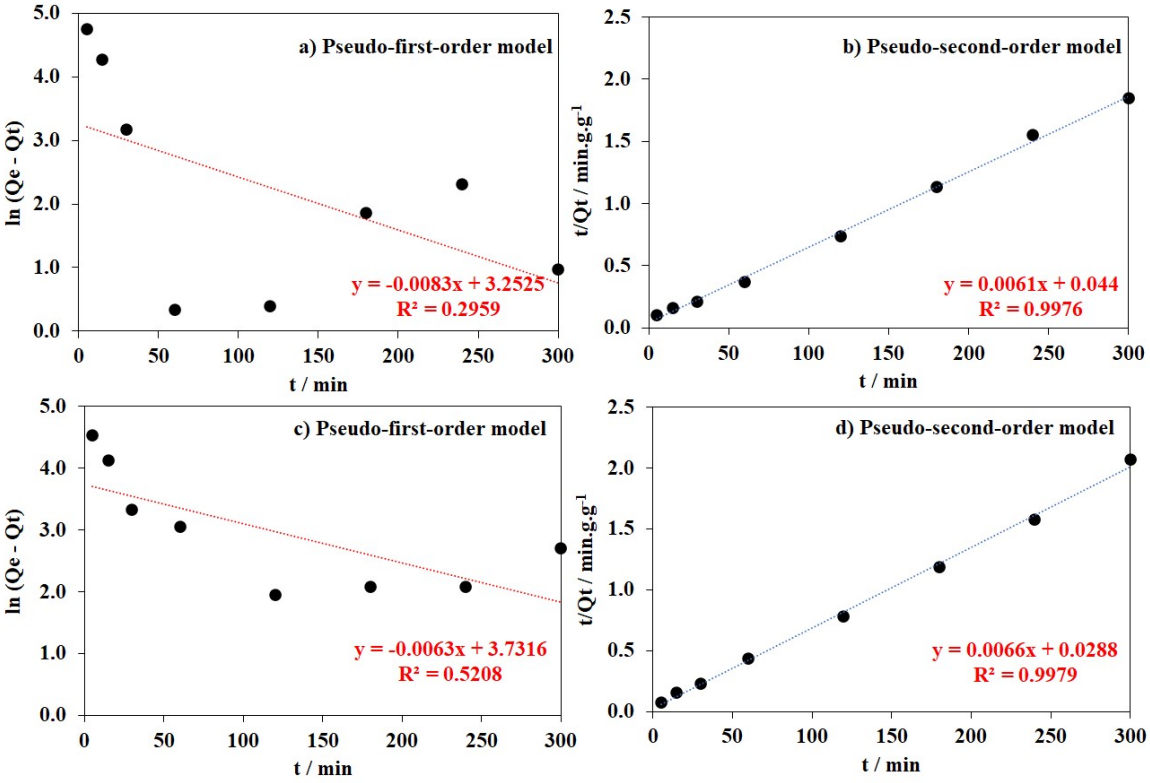

Figure S3. Pseudo first-order and second-order model of Cr (VI) anion adsorption processes as employing MOF-808-OH (a and b) and MOF-808-NH_2 (c and d).

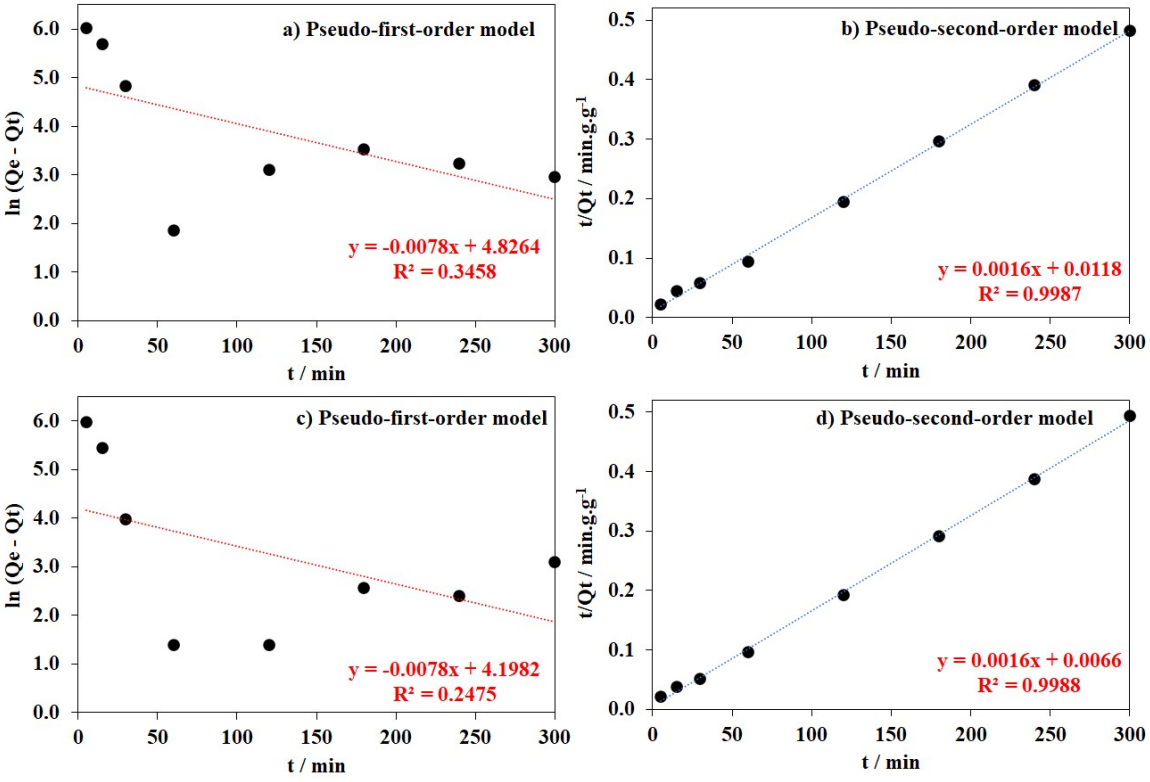

Figure S4. Pseudo first-order and second-order model of sunset yellow adsorption processes as employing MOF-808-OH (a and b) and MOF-808-NH_2 (c and d).

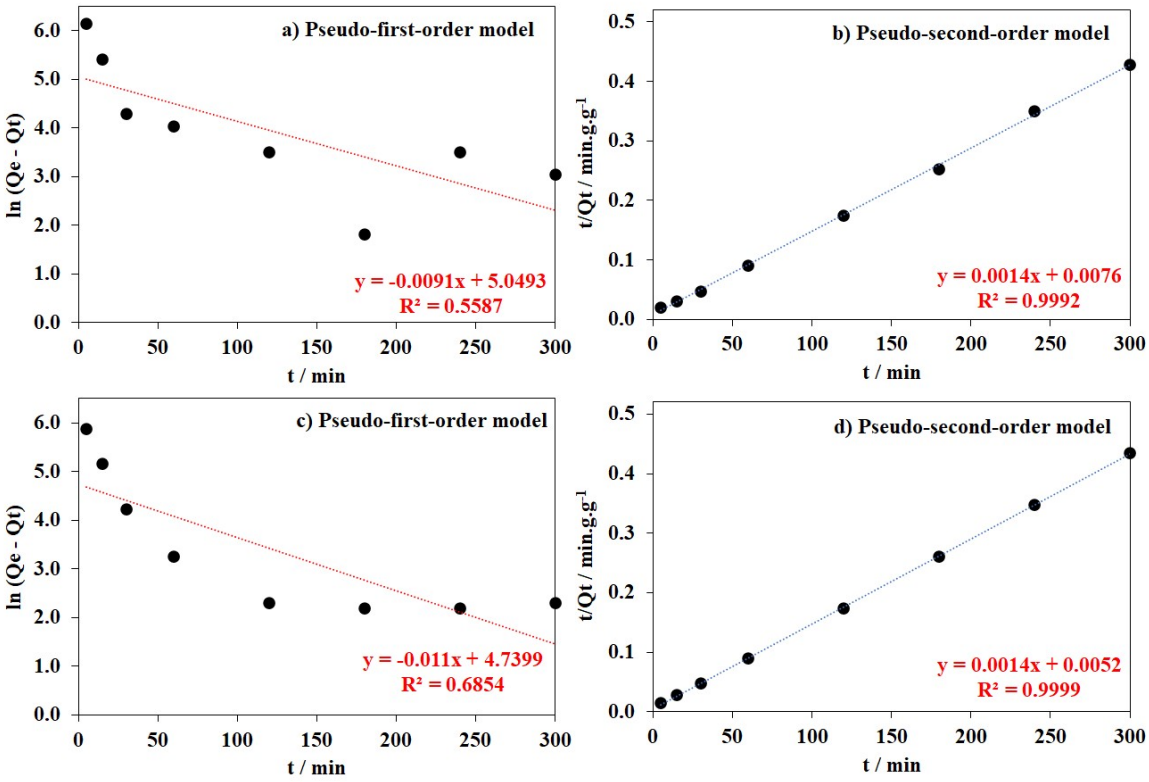

Figure S5. Pseudo first-order and second-order model of methyl orange processes as employing MOF-808-OH (a and b) and MOF-808-NH_2 (c and d).

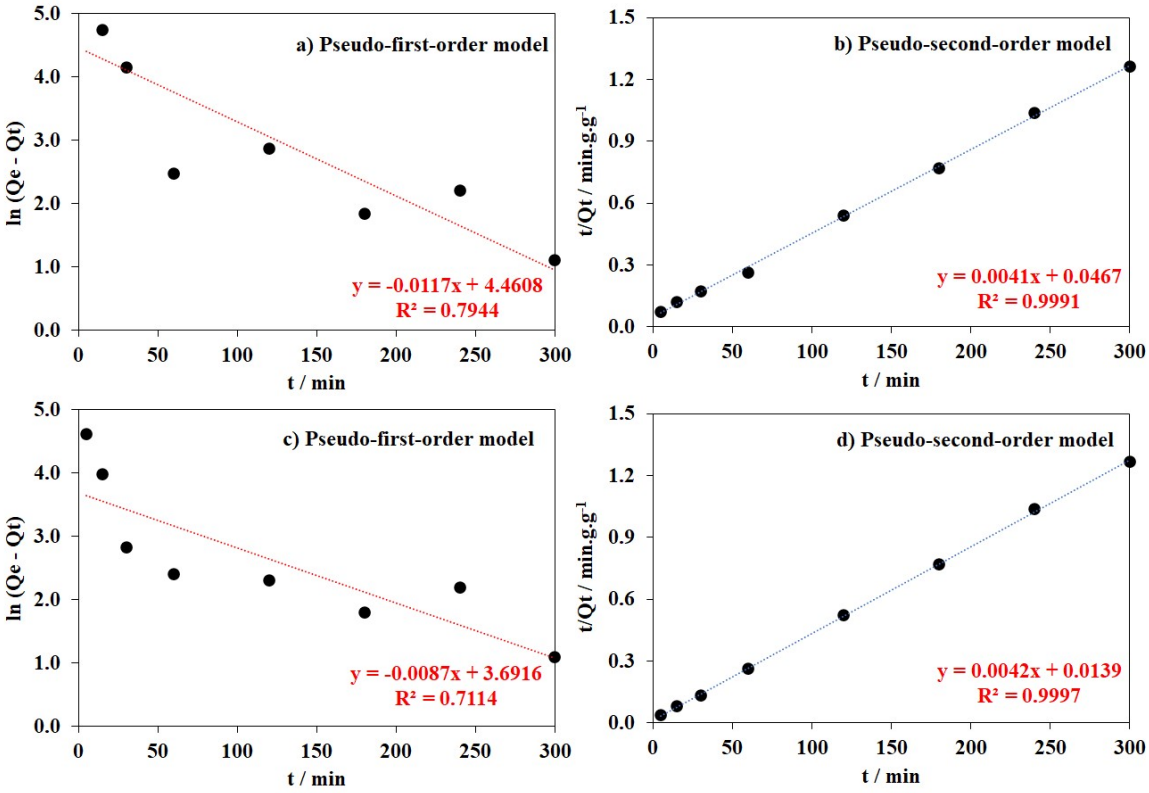

Figure S6. Pseudo first-order and second-order model of methyl blue processes as employing MOF-808-OH (a and b) and MOF-808-NH_2 (c and d).

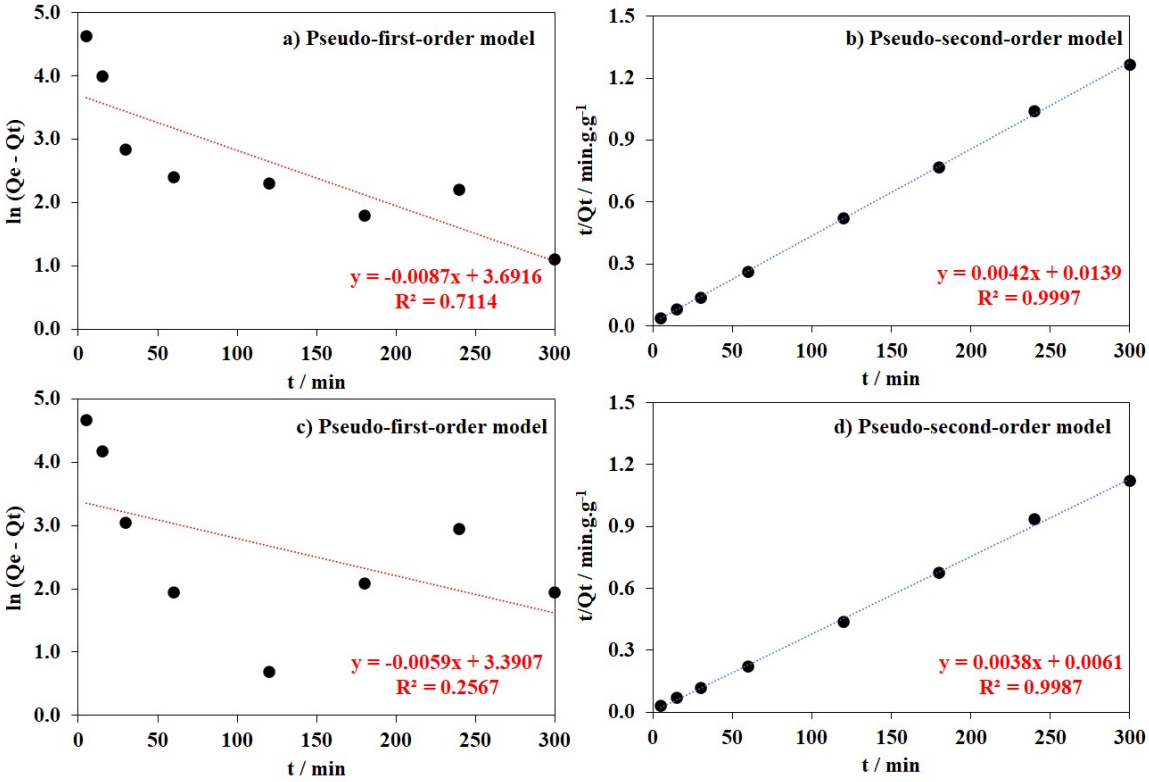

Figure S7. Pseudo first-order and second-order model of malachite green processes as employing MOF-808-OH (a and b) and MOF-808-NH_2 (c and d).

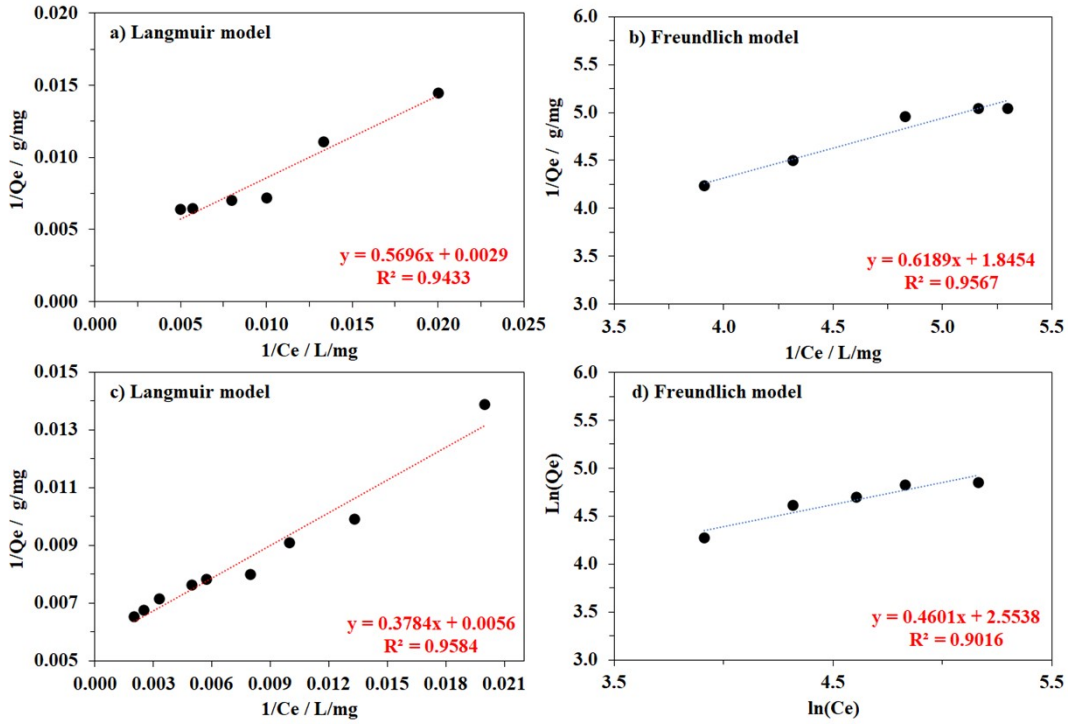

Figure S8. Dichromate adsorption isotherms of the MOF-808-OH (a and b) and MOF-808-NH_2 (c and d) fitting by Langmuir model and Freundlich model.

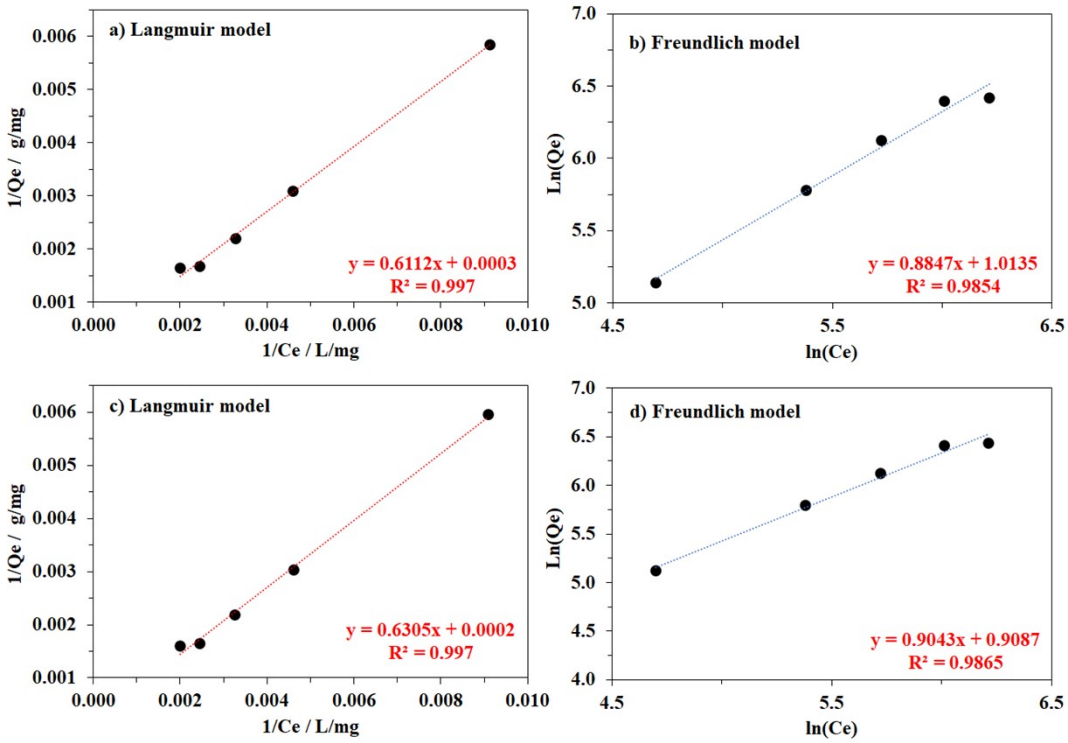

Figure S9. Sunset yellow adsorption isotherms of the MOF-808-OH (a and b) and MOF-808-NH_2 (c and d) fitting by Langmuir model and Freundlich model.

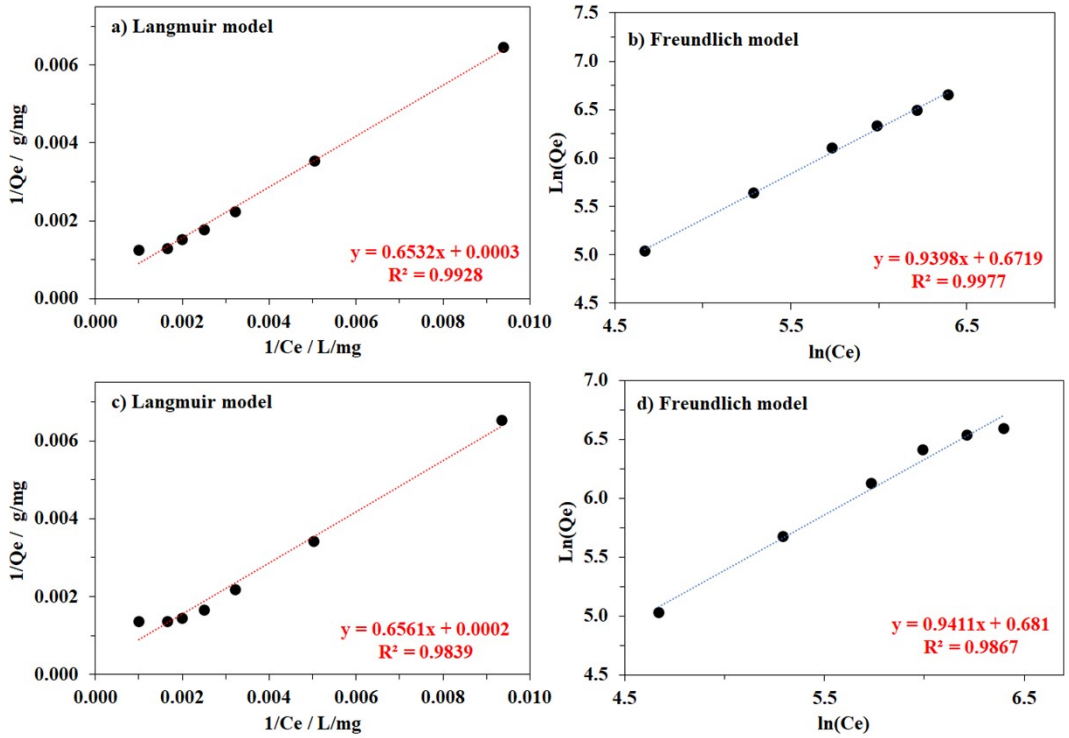

Figure S10. Methyl orange adsorption isotherms of the MOF-808-OH (a and b) and MOF-808-NH_2 (c and d) fitting by Langmuir model and Freundlich model.

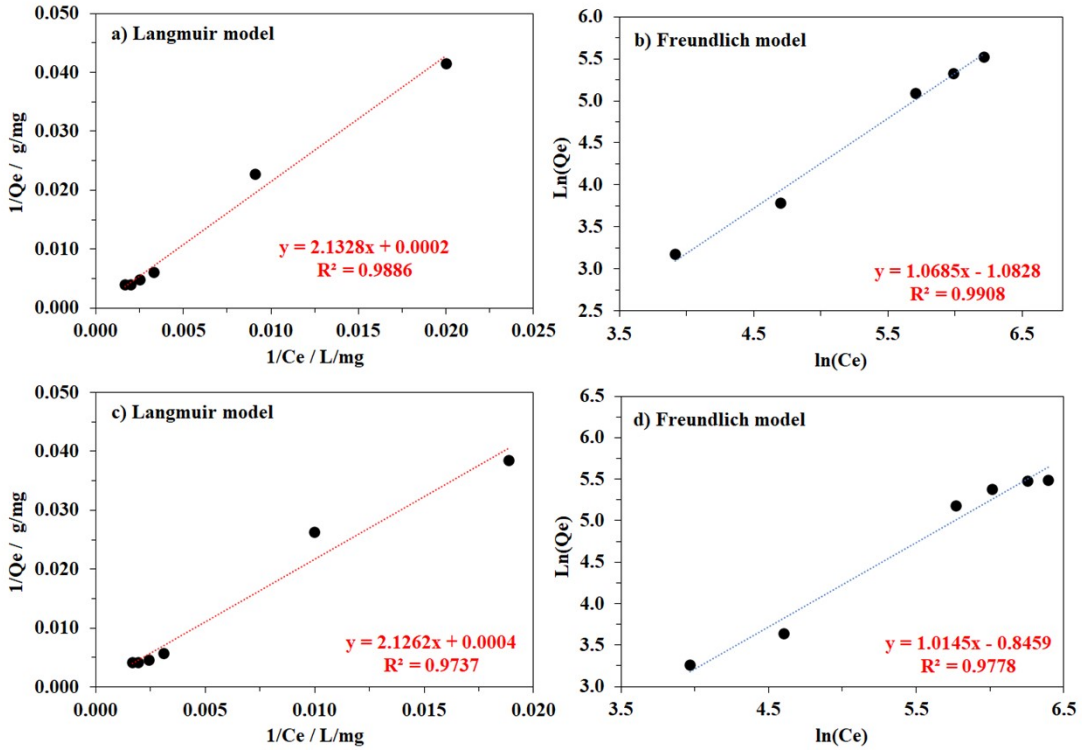

Figure S11. Methyl blue adsorption isotherms of the MOF-808-OH (a and b) and MOF-808-NH_2 (c and d) fitting by Langmuir model and Freundlich model.

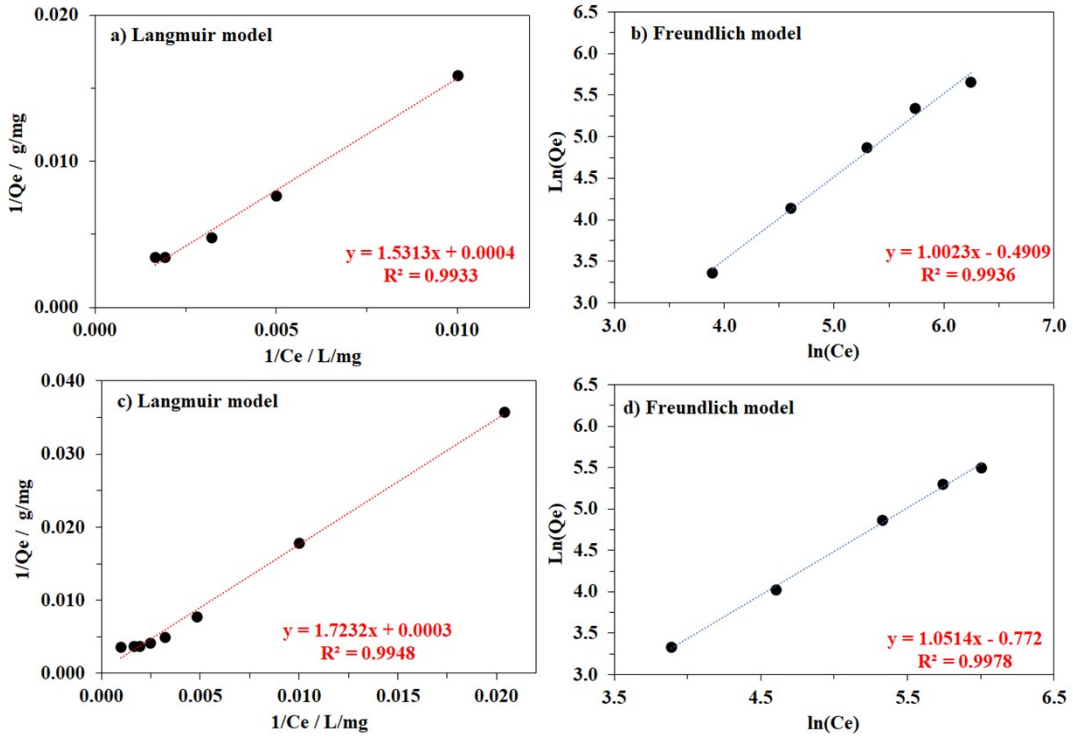

Figure S12. Malachite green adsorption isotherms of the MOF-808-OH (a and b) and MOF-808-NH_2 (c and d) fitting by Langmuir model and Freundlich model.

Table S2. Isotherm parameters of Langmuir and Freundlich models for adsorption processes of MOF-808-OH and MOF-808-NH_2

N.	Sample	Langmuir						Freundlich					
		MOF-808-OH			MOF-808-NH_2			MOF-808-OH			MOF-808-NH_2		
		K_L (L/mg)	Q_L (mg/g)	R^2	K_L (L/mg)	Q_L (mg/g)	R^2	n	K_F (L/g)	R^2	n	K_F (L/g)	R^2
1	Cr(VI) anion	0.0051	346	0.953	0.0148	179	0.958	1.62	6.33	0.957	2.17	12.86	0.902
2	SY	0.0004	3797	0.997	0.0003	5434	0.997	1.13	2.76	0.985	1.11	2.48	0.987
3	QY	0.0005	3321	0.980	0.0006	2636	0.984	1.02	1.65	0.995	1.04	1.83	0.999
4	MO	0.0004	3759	0.993	0.0004	4060	0.984	1.06	1.96	0.998	1.06	1.98	0.998
5	MB	0.0001	16170	0.988	0.0002	2386	0.974	0.94	0.34	0.991	0.99	0.43	0.978
6	MG	0.0002	2755	0.993	0.0002	2883	0.995	0.99	0.61	0.994	0.95	0.46	0.998

Table S3. Recycling tests of defective MOF-808 analogues as adsorbents for removing Cr (VI) anions, sunset yellow (SY), quinoline yellow (QY), methyl orange (MO) from aqueous solution

Adsorbent	**MOF-808-OH**				**MOF-808-NH_2**			
Adsorbate	**Cr(VI) (mg/g)**	**SY (mg/g)**	**QY (mg/g)**	**MO (mg/g)**	**Cr(VI) (mg/g)**	**SY (mg/g)**	**QY (mg/g)**	**MO (mg/g)**
1st run	164	612	701	659	153	626	702	690
2nd run	161	605	687	650	151	615	691	673
3rd run	159	595	680	641	142	608	679	663
4th run	151	588	671	636	139	599	675	659
Capacity loss (%)	7.9	3.9	4.3	3.5	9.2	4.3	3.8	4.5